Morphological description of colour images for content-based image retrieval

Erchan Aptoula, Sébastien Lefèvre

Morphological Description of Color Images for Content-Based Image Retrieval

Erchan Aptoula and Sébastien Lefèvre

***Abstract*—Placed within the context of content-based image retrieval, we study in this paper the potential of morphological operators as far as color description is concerned, a booming field to which the morphological framework, however, has only recently started to be applied. More precisely, we present three morphology-based approaches, one making use of granulometries independently computed for each subquantized color and two employing the principle of multiresolution histograms for describing color, using respectively morphological levelings and watersheds. These new morphological color descriptors are subsequently compared against known alternatives in a series of experiments, the results of which assert the practical interest of the proposed methods.**

***Index Terms*—Color description, content-based image retrieval (CBIR), granulometry, mathematical morphology (MM), multiresolution histogram.**

I. Introduction

THE first foundations of mathematical morphology (MM) were laid down during the sixties, within the context of stereology related projects aiming to describe iron ore properties [1] and porous media [2]. Hence, visual content description can be considered as one of the initial goals, that guided the research efforts leading eventually to the development of the entire morphological framework as it is known today [3].

Since that first period the potential of MM for feature extraction and content description has been demonstrated in various fields, ranging from biomedical applications [4] to remote sensing [5], [6]. The topic of general purpose content-based image retrieval (CBIR), however, with the exception of highly application specific cases (e.g., hematological cell classification [7]), has been left relatively unexplored. At the end of the inception years of CBIR, this has started to change. Rather direct applications of classical morphological operators, such as pattern spectra [8], multiscale segmentations [9], combinations with already known descriptors (Gabor filters and watershed based segmentation [10]) as well as novel morphological approaches [11] are becoming more frequent. Nevertheless, to the best of the authors' knowledge no extensive study has yet been carried out.

Manuscript received September 25, 2008; revised June 14, 2009. First published July 10, 2009; current version published October 16, 2009. The associate editor coordinating the review of this manuscript and approving it for publication was Dr. Laurent Younes.

The authors are with the LSIIT, UMR 7005 CNRS/University Louis Pasteur—Strasbourg, Pôle API, Bd Brant, BP 10413, 67412 Illkirch cedex, France (e-mail: aptoula@lsiit.u-strasbg.fr; lefevre@lsiit.u-strasbg.fr).

Color versions of one or more of the figures in this paper are available online at http://ieeexplore.ieee.org.

Digital Object Identifier 10.1109/TIP.2009.2027363

Besides the relative popularity of CBIR in the image processing community, the motivation for considering morphological operators in order to tackle this problem, is mainly due to the inherent capacity of this framework to exploit spatial pixel relationships. Based on this concept, in this paper we focus on color description, and study the potential of morphological operators for content description within this context. Why color? Because, although it is certainly not the most important visual quality of image data when it comes to semantic retrieval, it still is one of the basic low level visual features, and as such it constitutes a good launching point for future work consisting of the development of more sophisticated morphological content decriptors, e.g., morphological color interest point detectors or other multiscale morphological approaches. More precisely, our contribution consists of three novel morphology based color descriptors, based on granulometries and multiresolution histograms in combination with color levelings and the watershed transform. All three proposed approaches are compared against known alternatives in a series of tests, that assert the practical interest of the morphological framework in this field.

We first provide in Section II a short overview of the application of MM to color images and its related issues as it is far from being straightforward. Then we focus on the development of morphology based color descriptors making use of granulometries and multiresolution histograms (Section III). Next we present the results of a series of comparative tests illustrating the interest of the proposed methods (Section IV), followed by concluding remarks (Section V).

II. Color Morphology

The extension of morphological operators to color and more generally to multivariate images is an open problem. Specifically, since the morphological framework is based on complete lattice theory [12], it is theoretically possible to define morphological operators on any type of image data, as long as a complete lattice structure can be introduced on the image intensity range. In other words, given the vector nature of color pixels, a vector ordering becomes necessary. Several approaches have been proposed with this purpose (e.g., marginal orderings, reduced orderings, conditional orderings, etc.), a comprehensive survey of which can be found in [13]. Prior to choosing a vector ordering, however, it is imperative to select a color space to work with.

A. Color Space

Here, we choose to follow the trend of the last years in the domain of color morphology, and employ a polar color space based on the notions of hue ($h \in [0, 2\pi]$), saturation ($s \in [0, 1]$) and luminance ($l \in [0, 1]$). More precisely, although most

polar color spaces are essentially a more intuitive description of the RGB color cube, several implementations exist e.g., HSV, HLS, HSI, etc. According to Hanbury and Serra [14], [15], the cylindrical versions of these spaces have serious inconsistencies and are inappropriate for quantitative color image processing. Hence, we make our color space choice in favor of the *improved HLS* space, which employs the original biconic version of HLS. This color space has been introduced in [16], [17] under the name LSH, and can be computed from the RGB space as

$$\begin{aligned} L_{\mathrm{LSH}} &= \frac{1}{3}(\max + \mathrm{med} + \min) \\ S_{\mathrm{LSH}} &= \begin{cases} \frac{3}{2}(\max - L_{\mathrm{LSH}}) & \text{if } L_{\mathrm{LSH}} \geq \mathrm{med} \\ \frac{3}{2}(L_{\mathrm{LSH}} - \min) & \text{if } L_{\mathrm{LSH}} \leq \mathrm{med} \end{cases} \\ H_{\mathrm{LSH}} &= k\left[\lambda + \frac{1}{2} - (-1)^{\lambda}\left(\frac{\max + \min - 2\mathrm{med}}{2S_{\mathrm{LSH}}}\right)\right] \end{aligned} \quad (1)$$

where $\max, \mathrm{med}$, and $\min$ denote respectively the maximum, median and minimum value of the transformed RGB triplet. k is the angle unit ($\pi/3$ for radians and 42 for 256 levels), whereas λ is set as 0 if $r > g \geq b$, 1 if $g \geq r > b$, 2 if $g > b \geq r$, 3 if $b \geq g > r$, 4 if $b > r \geq g$, and 5 if $r \geq b > g$.

One of the most important drawbacks of the cylindrical HLS space is the unintuitive definition of saturation. Specifically, it is possible to have maximized saturation values for zero luminance. This inconvenience, as well as the dependence of saturation on luminance are remedied with the LSH space, where the maximal allowed value for saturation is limited in relation to luminance. Therefore, in order to benefit from the advantages of polar spaces in the context of multivariate morphology, the ordering of LSH color vectors is required.

B. Color Ordering

As to the issue of color ordering, it is nontrivial since it is tied both to the problem of multivariate ordering as well as to the subjective notion of color. In order to realize our choice of color ordering among the available rich variety, we focused on two criteria, first its theoretical stability and second its suitability to the color space under consideration. For these reasons, we have chosen to use primarily the lexicographical ordering (i.e., a total ordering leading to theoretically valid morphological operators) and more specifically its quantization based variant [18], which renders it not only more flexible but takes into account the particular relations among the dimensions of LSH as well (e.g., the redundancy of hue when a pixel is not saturated "enough").

More precisely, the quantization based lexicographical ordering is based on the standard lexicographical cascade, which is defined by

$$\begin{aligned} \forall \mathbf{v}, \mathbf{v}' \in \mathbb{R}^n, \mathbf{v} <_L \mathbf{v}' \Leftrightarrow \exists i \in \{1, \ldots, n\}, \\ (\forall j < i, v_j = v'_j) \wedge (v_i < v'_i) \end{aligned} \quad (2)$$

It is applied on the color vectors of LSH, where the importance of saturation is maximized for medium levels of luminance, whereas hue is of practical importance only for relatively high levels of saturation. Thus, we conform here to previous works [13] and use $L \rightarrow S \rightarrow H$ in the lexicographical cascade, where the first two components are subquantized nonuniformly according to functions modeling the interchannel relations of the color space

$$\begin{aligned} &\forall \mathbf{v}_1 = (l_1, s_1, h_1), \mathbf{v}_2 = (l_2, s_2, h_2) \in [0, 255]^3 \\ &\mathbf{v}_1 < \mathbf{v}_2 \Leftrightarrow [l'_1, s'_1, h_1]^T <_L [l'_2, s'_2, h_2,]^T \end{aligned} \quad (3)$$

In particular, we have used the exact configuration presented in [18] concerning luminance (l) and saturation (s) to produce quantized luminance (l') and saturation (s') (note that any eventual equivalences among distinct color vectors may be avoided by using the lexicographical cascade once more with the original pixel values). As to the hue, however, since it is a 2π-periodical angular value, it has been decided to use a reference based hue ordering [19]

$$\forall h, h' \in [0, 2\pi], h \leq h' \Leftrightarrow h' \div h_0 \leq h \div h_0 \quad (4)$$

where hues are ordered with respect to their distance to a reference value h_0 (to be defined depending on the application), with the closer ones being considered greater. As to the distance measure, it is defined as [19]

$$\begin{aligned} &\forall h, h_0 \in [0, 2\pi] \\ &h \div h_0 = \begin{cases} |h - h_0| & \text{if } |h - h_0| < \pi \\ 2\pi - |h - h_0| & \text{if } |h - h_0| \geq \pi \end{cases}. \end{aligned} \quad (5)$$

Therefore, equipped with the ordering of (3) one can compute the vector extrema by means of $\inf_v$ and $\sup_v$, necessary for the definition of the basic morphological operators of vector erosion $(\boldsymbol{\varepsilon}_b)$ and dilation $(\boldsymbol{\delta}_b)$

$$\boldsymbol{\varepsilon}_b(\mathbf{f})(\mathbf{x}) = \underset{\mathbf{s} \in b}{\inf_v} \{\mathbf{f}(\mathbf{x} + \mathbf{s})\} \quad (6)$$

$$\boldsymbol{\delta}_b(\mathbf{f})(\mathbf{x}) = \underset{\mathbf{s} \in b}{\sup_v} \{\mathbf{f}(\mathbf{x} - \mathbf{s})\} \quad (7)$$

from the combinations of which more sophisticated operators may be obtained. Now let us proceed to the developments of morphological operators for color images aiming to describe color content.

III. Morphological Description of Color Images

Color is widely regarded as one of the most expressive visual features [20], and as such it has been extensively studied in the context of CBIR, thus leading to a rich variety of descriptors [21]. Similarly to texture and shape, it is relatively hard to establish the exact description of color content. One has to ask, given a color image, which notions describe the concept of color within it. Considering the existing amount of work on this topic, and the multitude of color descriptors employed in commercial and research systems, one can narrow down the type of information extracted from them to the following.

- The presence (or absence) of a particular color (e.g., red and blue).
- The relative amount in which a particular color is present (e.g., 80% red and 20% blue).
- The size distribution of each color (e.g., one large patch of red and multiple small patches of blue).
- The relative spatial position of each color with respect to others (e.g., red at left and blue at right).

The last of the aforementioned four notions is of use only in cases where the relative position of color components is of semantic importance. Such an assumption makes possible to use (multiscale) segmentation-based approaches where the image is represented as a set of regions through a graph (or tree) structure. In this very particular context, mathematical morphology is a possible solution [9]. An example of images where this notion is relevant is the following: in the case of beaches, the sand (brown and/or gray) is next to the sea (blue and green), above which is the sky (blue and/or gray). Of course there are also numerous other objects for which relative positions cannot be *a priori* determined, for instance accordions, books, etc. Consequently, one can understand why the vast majority of existing work on this topic concentrates on the first three notions in order to describe color content.

Any attempt on color description, however, has to address certain issues first. These are the choice of color space and quantization levels, as well as the variations due to different illumination conditions. The choice of color space is of vital importance, as it has a direct effect on channelwise correlation, and consequently on the effectiveness of the resulting feature vectors. Although perceptual spaces (e.g., $\mathrm{L^*a^*b^*}$, $\mathrm{L^*u^*v^*}$) are considered to better model the human perception of color, comparative studies have shown phenomenal color spaces to outperform them in combination with several descriptors [22].

As the standard number of colors in everyday digital images is usually in the order of millions, color specific approaches naturally lead to excessively large feature vectors; hence, color subquantization (i.e., quantization to fewer levels) is a common practice. The exact number of levels along with their uniformity, however, depend strongly on the chosen color space. For instance while 4 colors per channel are preferred for RGB (i.e., 4-4-4, 64 colors), 16-4-4 is usually used with HSV [20], [23]. The question of choosing the optimal quantization model and number of levels can be considered as a search for the optimal compromise between feature vector size and effectiveness.

Another significant obstacle in color description is the one caused by color variations due to different illumination conditions. Even with exactly the same object and viewing angle, changing only the illumination source may lead to totally different color distributions. One can counter this effect, either by means of an appropriate transformation, like histogram equalization (Fig. 1) [24] or by subquantizing strongly the luminance component in order to reduce its influence [25].

Despite the absence of previous work on the morphological characterization of color distributions, we believe that morphological options possess the potential to contribute to all three stages of it, specifically preprocessing (e.g., image simplification), processing (e.g., feature extraction) and postprocessing (e.g., descriptor refinement). In the light of the aforementioned color description principles, we present three global/holistic approaches for the description of color based on morphological operators, that are subsequently compared against known alternatives.

A. Color Specific Granulometry (CSG)

Since the first two requirements for describing color content can be trivially obtained through an histogram, the main problem to address is finding a means to describe the spatial/size distribution of colors. To this end, an important part of the existing methods follows a color specific approach, where each color is described independently, either by means of an autocorrelogram or some other spatial histogram extension, each color bin is associated additionally with a spatial description. That is why it has been decided here not to employ a vector processing strategy, and instead focus on each quantized color separately using granulometry as our description tool. Besides, CBIR oriented color granulometries have already been reported, such as the one by Angulo and Serra [26], where they are computed marginally in the RGB space and the one by Louverdis *et al.* [27], defined in HSV using a lexicographical ordering, which, however, ignores the hue component's periodicity.

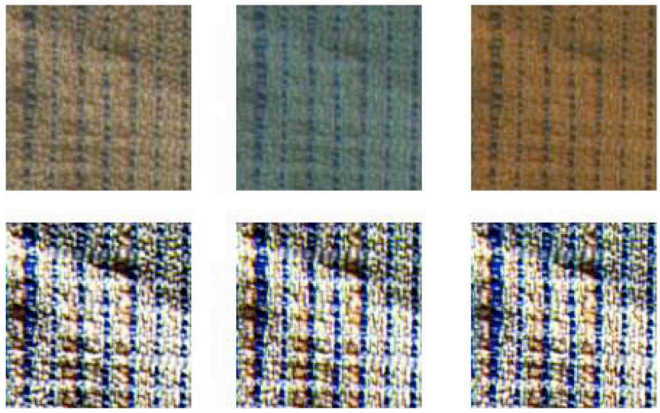

Fig. 1. In the first row, a texture example from the Outex14 texture database under three different illumination sources (left to right, 2856 K incandescent CIE A, 2300 K horizon sunlight and 4000 K fluorescent TL84) and in the second row, the same images after the application of a channelwise histogram equalization in RGB.

Intuitively, we choose to associate each color of the input with its corresponding granulometric curve, since it is considered as the morphological tool by default for the description of size distributions [28]. In particular, this operator consists in studying the amount of image detail removed by applying morphological openings γ_λ and/or closings ϕ_λ of increasing size λ. The volumes (i.e., sum of graylevel pixel values) of the opened (or closed) images are then plotted against λ, or more usually their discrete derivative $\mathrm{Vol}(\gamma_\lambda - \gamma_{\lambda+1})$, i.e., *pattern spectrum*.

In the present case, given a color image $\mathbf{f}$ with possible colors in $\{c_i\}_{1\leq i\leq m}$, a graylevel image f_{c_i} for each c_i is computed, where every pixel $f_{c_i}(x,y)$ denotes the distance of $\mathbf{f}(x,y)$ to c_i

$$\forall (x,y), f_{c_i}(x,y) = d(\mathbf{f}(x,y), c_i) \tag{8}$$

where d represents a color metric suitable for the color space under consideration, e.g., the Euclidean distance for perceptually uniform spaces. Next we compute the granulometric curve of f_{c_i} using closings by reconstruction. To explain, closing by reconstruction is a high level morphological operator which can be expressed in the digital case in terms of geodesic erosions. Geodesic erosion $\varepsilon_g^{(1)}(f)$ and dually geodesic dilation $\delta_g^{(1)}(f)$ are operations involving two images, a marker image f and a mask g, where the first is processed conditionally to the second

$$\varepsilon_g^{(1)}(f) = \varepsilon(f) \vee g \tag{9}$$

$$\delta_g^{(1)}(f) = \delta(f) \wedge g \tag{10}$$

where ε and δ are the erosion and dilation by the neighborhood of the origin. Both operators can be further applied successively as follows:

$$\psi_g^{(n+1)}(f) = \psi_g^{(1)}\left(\psi_g^{(n)}(f)\right) \tag{11}$$

hence, by repeating them until stability (i times, $\psi_g^{(i)}(f) = \psi_g^{(i+1)}(f)$) one can realize respectively a reconstruction by erosion and a reconstruction by dilation

$$R_g^{\varepsilon}(f) = \varepsilon_g^{(\infty)}(f) \tag{12}$$

$$R_g^{\delta}(f) = \delta_g^{(\infty)}(f) \tag{13}$$

which reach stability after a finite number of steps. Consequently, one can define closing by reconstruction with a structuring element (SE) B

$$\phi_{R,B}(f) = R_g^{\varepsilon}[\delta_B(f)] \tag{14}$$

which we use in combination with SE of various sizes, in order to compute the granulometric curve of f_{c_i} that describes color c_i

$$\mathrm{h}_f^k(c_i) = \mathrm{Vol}(\phi_{R,B_k}(f_{c_i}))/\mathrm{Vol}(f_{c_i}) \tag{15}$$

$$\forall c_i, \mathrm{h}_f(c_i) = \left\{\mathrm{h}_f^k(c_i) \,|\, k \in \{1,\ldots,n\}\right\} \tag{16}$$

where B_k is the SE of size k to be used in the closing by reconstruction, and Vol denotes the image volume (i.e., sum of graylevel pixel values of each f_{c_i}). Consequently, the final feature vector is formed by the concatenation of all $h_f(c_i)$, leading to a descriptor of size $n \times m$. The reason for using a closing instead of an opening is because the regions representing colors similar to the one under consideration will be at minimal distance, hence, dark, whereas the choice of a reconstruction based operator is justified by the reports concerning the improvement of performance that it brings in the context of content description [29].

Moreover, granulometries, similarly to correlograms, are invariant with respect to spatial position [30], and provide a description of the size distribution of their content. Applying them directly on the input image results in a fairly effective shape descriptor [8]. By applying them "marginally" for each possible color, one can distinguish for instance a connected "large" patch of color c_i, from a number of smaller components of the same color. As to its similarity comparison, we find it pertinent to use an approach similar to the relative L_1 distance based measure of correlograms [31]

$$d_{\mathrm{CSG}}(\mathbf{f},\mathbf{f}') = \sum_{1\le i\le m, 1\le k\le n} \frac{|h_f^k(c_i) - h_{f'}^k(c_i)|}{1 + h_f^k(c_i) + h_{f'}^k(c_i)}. \tag{17}$$

An illustrative example of CSG is given in Fig. 2, where the curves obtained for three colors of different size distribution are shown. Possible extensions to the definition of (16) could include using multivariate granulometries (e.g., size-shape) [32], as well as higher order statistical measures instead of the volume [33].

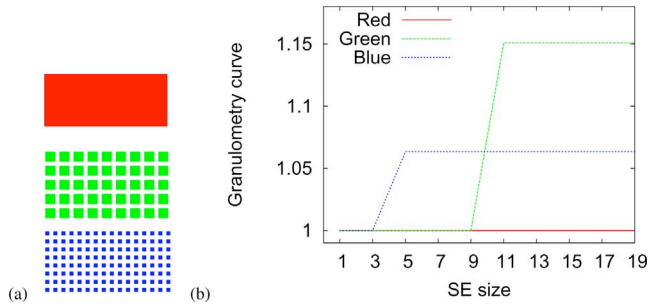

Fig. 2. Input image (a) and the granulometric curves (b) coresponding to red, green and blue, obtained by processing the distance image of (a) computed using an Euclidean distance in RGB.

B. Multiresolution Histograms in the Leveling Scale-Space (MHL)

Color histograms remain simple yet effective tools since the early days of CBIR [34], with positive properties such as invariance to geometric transformations. As they are capable of providing the first two elements required for the description of color, their foremost drawback is the lack of any spatial information. To this end, several extensions have been proposed [35], [21]; among which one particular approach is using multiple resolutions, that has proven itself to be able to capture effectively color content [36], [37]. Multiresolution decomposition has been achieved by means of Gaussian filters [36], Gabor filters [38] as well as wavelets [39]. For an in-depth study on this topic the reader can consult [36]. Morphological scale spaces, however, have not yet been used to this end, despite being used for other multiscale image representations (e.g., related to segmentations [9]).

Scale-spaces based on morphological levelings have been studied in particular by Meyer and Maragos [40], where the useful properties of levelings, such as contour preservation and invariance to translation and rotation among others have been mentioned. This formulation later on has been used for optimal scale selection by exploiting the property of maxima propagation within levelings [41], and for multiscale image description through segmentation tree [9]. Here, however, we propose to employ this scale space for the description of color distribution by means of multiresolution histograms. Before proceeding any further, let us recall the relative definitions. Levelings are powerful morphological operators representing a subclass of connected operators, that work on a reference image $\mathbf{f}$ and a marker image $\mathbf{g}$. The marker image is modified in such a way that it becomes the leveling $\mathbf{g}' = \lambda(\mathbf{f},\mathbf{g})$ of $\mathbf{f}$. From an implementational point of view, the expression

$$\mathbf{g}' = [\mathbf{f} \wedge \boldsymbol{\delta}(\mathbf{g})] \vee \boldsymbol{\varepsilon}(\mathbf{g}) \tag{18}$$

is iterated until idempotence, although more efficient algorithms also exist [42].

At this point two issues need to be addressed, first the extension of levelings to color images, as well as the formulation of a scale-space. The first has been studied by Gomila and Meyer [43] and by Angulo and Serra in [44], where different orderings and color spaces have been tested. It consists in replacing the scalar morphological as well as binary operators of (18) by their

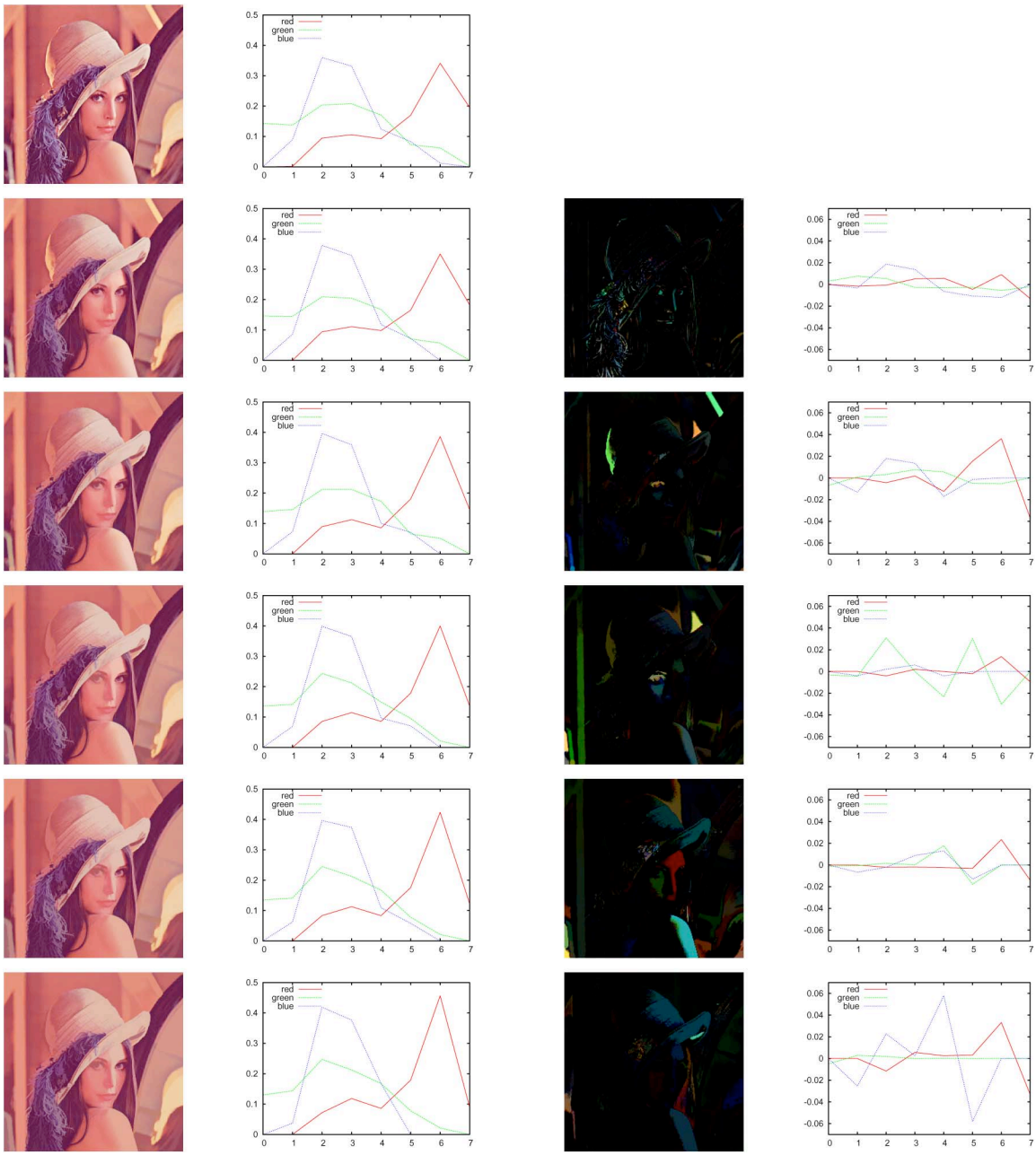

Fig. 3. From top to bottom: Original Lenna image and its vectorly leveled versions using (18) and (19), with marker images obtained using alternating sequential filters (ASF) of increasing size 3, 5, 7, 9, and 11. Each line contains (from left to right): the (leveled) color image (a) and its corresponding 8-bin RGB color normalized histograms (b), the differences with the finer image (i.e., from previous line or resolution) emphasized with contrast stretch (c) and considering its color normalized histograms (d). (This figure is best viewed in color).

vector versions. As to the second, multiple methods are possible such as using a family of extensive and anti-extensive operators within (18) or a family of marker images $\{\mathbf{g}_i\}$ that lead to progressively simplified images

$$\begin{aligned} &\text{For resolution } i \in \{1, \ldots, n\} \\ &\mathbf{g}'_0 = \mathbf{f} \quad \text{and} \quad \mathbf{g}'_i = \lambda(\mathbf{f}, \mathbf{g}_i). \end{aligned} \tag{19}$$

Of course, a variety of filters may be used in order to obtain the marker images, including alternating sequential filters (ASF), Gaussian or even anisotropic diffusion filters, that according to the study in [45] provide the best quantitative performance in terms of noise reduction capacity. An example of successive color levelings applied on the Lenna image (256×256 pixels) is given in Fig. 3(a), where the multiple marker images are obtained through vectorial ASF (with opening first) of various sizes i expressed as

$$\mathrm{ASF}_i(\mathbf{f}) = \phi_i \gamma_i \ldots \phi_2 \gamma_2 \phi_1 \gamma_1(\mathbf{f}) \tag{20}$$

where ϕ_i and γ_i represpectively represent the closing and opening of size i. Using a smoother marker leads to larger flat regions and results in a removal of more details as shown in Fig. 3(c), where contrast has been stretched for visualization purpose. Moreover, the leveling process modifies the corresponding color histograms as illustrated in Fig. 3(b), which contains normalized histograms. Differences between color histograms at successive resolutions (i.e., when computed from successive leveled images) are emphasized in Fig. 3(d). These differences can reach up to 4000 pixels for a given quantized color and correspond to the large areas shown in Fig. 3(c).

Given n resolutions, one can then compute the color histogram of size m of each g'_i and concatenate them in order to form the feature vector of size $n \times m$. Moreover, the histogram differences may also be used. As to the similarity measure, while the histogram intersection is of course the standard choice, a weighting factor may also be added, following the principle of a *pyramid match* [46]. In detail, since highly simplified images are bound to be more alike than the lower resolutions where more image detail is preserved, it makes sense to weight the corresponding histogram intersections. For instance, given $H(\mathbf{f}) = \{H_i(\mathbf{f})\}_{0 \le i \le n}$ and $H(\mathbf{h}) = \{H_i(\mathbf{h})\}_{0 \le i \le n}$, the multiresolution histogram families for two images $\mathbf{f}$ and $\mathbf{h}$, respectively, their weighted distance d_w would become

$$d_w(H(\mathbf{f}), H(\mathbf{h})) = \sum_{i=0}^{n} \frac{1}{2^i} \sum_{j=1}^{m} \min\{H_{ij}(\mathbf{f}), H_{ij}(\mathbf{h})\} \tag{21}$$

where H_{ij} denotes the jth histogram bin of resolution i. Further refinement may be achieved by modifying the bin width at each resolution.

C. Multiresolution Histograms Based on Watersheds (MHW)

Another morphological tool that may be used in order to boost the spatial sensitivity of the standard color histogram is the watershed transform. This powerful operator represents the foremost morphological approach to the problem of image segmentation. Although fully automatic, it is relatively sensitive to image noise, hence leading often to oversegmented results unless some form of smoothing is applied first. Nevertheless, the regions that are formed represent uniform areas in terms of spectral content or "flat" in topological terms. Here we propose to use this operator in order to produce the different image resolutions that are to be used in order to construct a multiresolution histogram. To do so we rely on multiple smoothed images, e.g., the leveled images presented in previous section. Let us notice, however, that it would have also been possible to involve multiscale watershed-based techniques (e.g., waterfalls [47], using contour saliencies [48], etc.) which produce directly segmentations at multiple resolutions, thus avoiding the need for multiple smoothed images.

In particular, given a color image $\mathbf{f}$, it is first smoothed relatively to resolution i and then segmented by means of the watershed transform, which leads usually to several regions. Then, the pixels of each region are associated with the representative color of that region. Several techniques may be involved to compute this representative color, among which we can cite: the average color (using a standard average function computed marginally on each component of the color space under consideration); the most dominant color (seeking for the main peak of the color histogram); the most homogeneous color (considering the color of the valley in the topographic surface, i.e., the pixel with minimum gradient value). Consequently, one can at this point compute the standard histogram taking into account the newly formed regions. Besides, using multiple resolutions means that the initial image will be further smoothed, hence leading to the formation of even larger flat regions, and, thus, we obtain a multiresolution representation of the input the histograms of which capture indirectly the spatial organization of its content. This procedure is further illustrated in Fig. 5. Consequently, the end feature vector is formed by the concatenation of the histograms of each resolution, thus leading to a size of $n \times m$, where n is the number of resolutions and m the number of bins of each histogram. As a similarity measure, we consider the pyramid match of (21) as adequate.

Although it appears as a straightforward approach, its implementation is hindered, however, by certain elements. First, there is the issue of a morphological color image segmentation [17]. The watershed transform is most often applied on a graylevel input representing the topographic relief of the image under consideration, usually its gradient, that is why an effective means of computing the color variations is necessary. To this end, we choose to combine the color channels by means of a channel-wise maximum of marginal gradients

$$\forall (l,s,h) \in [0,1]^3 \rho_{\mathrm{LSH}}(l,s,h) = \max\{\rho(l), \rho(s), \rho_H(h,s)\} \tag{22}$$

where $\rho = f - \varepsilon(f)$ is the standard internal morphological gradient, chosen instead of its alternatives based on experimental observations. Although the components of the polar color spaces are highly intuitive, their combination is relatively problematic. In particular, hue is of no importance if saturation is "low," while the biconic shape of the color space assures that no high saturation levels exist, if luminance is not "high enough." Hence, the hue gradient needs to be weighted with a coefficient that has a strong output only when both compared saturation values are "sufficiently high". Besides, on the contrary of the other two components, it has been observed that the $\max - \min$ form provides visually superior results with the hue, hence leading us to use the following expression:

$$\rho_H(h,s) = \max_{i \in B}\{j(s,s_i) \times h \div h_i\} - \min_{i \in B}\{j(s,s_i) \times h \div h_i\} \tag{23}$$

where B is the local 8-neighborhood, $\div$ the hue distance defined in (5) and $j(\cdot,\cdot)$ a double sigmoid controling the transition from "low" to "high" saturation levels

$$j(s_1,s_2) = \frac{1}{(1+\exp(\alpha \times (s_1 - \beta))) \times (1+\exp(\alpha \times (s_2 - \beta)))} \tag{24}$$

where the slope $\alpha = -10$ and the offset $\beta = 0.5$.

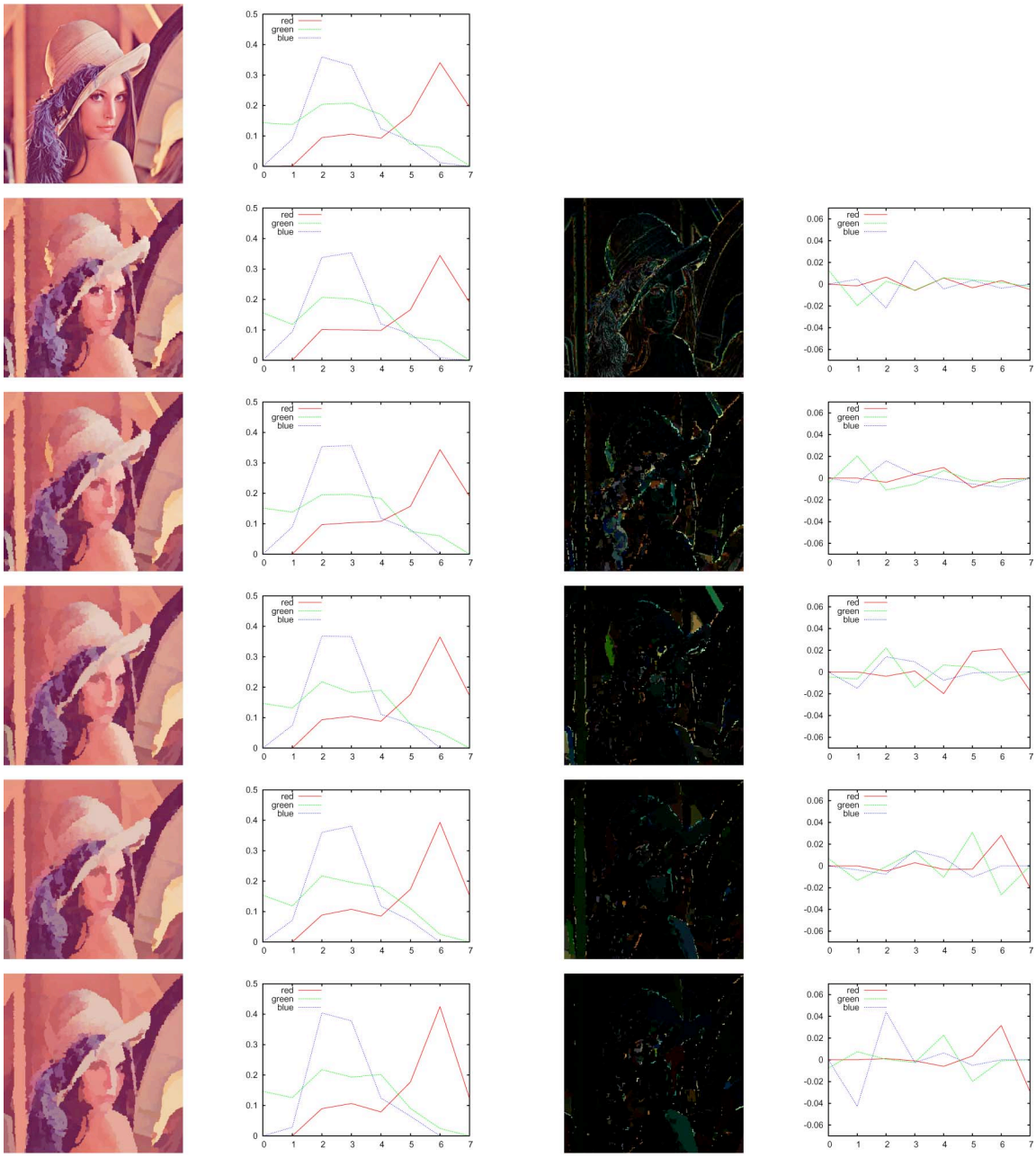

Fig. 4. From top to bottom: Original Lenna image and the results obtained after the watershed computation on the levelings of Fig. 3(a), where pixel values have been replaced by the valley color of each basin. Each line contains (from left to right): the resulting color image (a) and its corresponding 8-bin RGB color normalized histograms (b), the differences with the finer image (i.e., from previous line or resolution) emphasized with contrast stretch (c) and considering its color normalized histograms (d). (This figure is best viewed in color).

Moreover, one also has to choose a means to compute the progressively smoothed versions of the input image. Here, we consider color levelings with this purpose, the marker images of which may be obtained with any of the options mentioned in Section III-B. Following the flattening realized by levelings, the flat regions will be easily detected by the watershed transform, that will also detect as regions all basin shaped areas that have not been flattened by levelings. Whether this nuance has a positive or negative effect on the operator's color content description capacity is a question to be answered experimentally in Section IV but we still provide here a comparison on the standard Lenna image. The application of the watershed transform on the computed gradient leads to the result shown in Fig. 4(a), whereas Fig. 4(b) shows their color normalized histograms. Similarly to the leveled images, interresolution differences are present though hard to observe. Thus, we also provide contrast-stretched visual and normalized histogram differences in Fig. 4(c) and (d), respectively. Here we consider the valley color as the representative color of each region, but let us notice that some other tests with average color provide very similar results.

To illustrate the difference between the two multiscale approaches (using levelings only or levelings followed by wa-

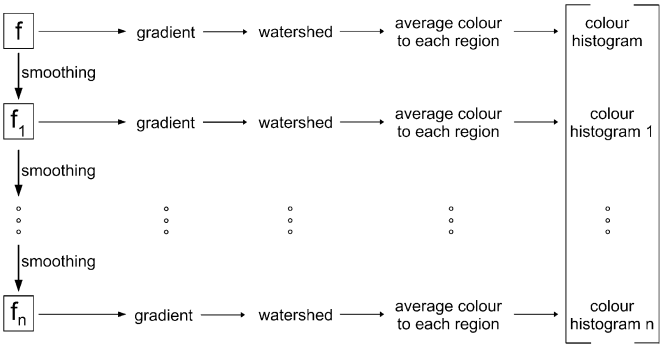

Fig. 5. Illustration of the steps required for forming the watershed transform based multiresolution histograms.

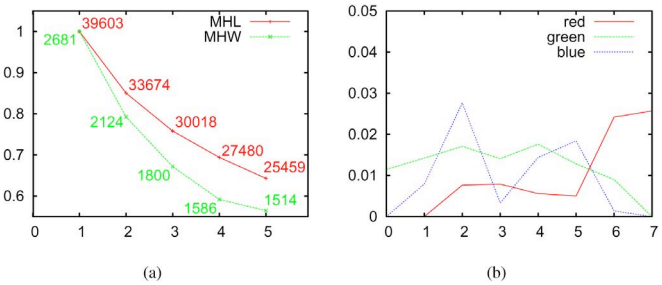

Fig. 6. Difference between multiresolution histograms using levelings only (MHL) and levelings followed by watersheds (MHW): (a) evolution of the color number at different image resolutions relatively to the first resolution, (b) average difference (among the different resolutions) between the three 8-bin RGB color normalized histograms obtained from MHL and MHW.

tersheds), we measure in Fig. 6(a) the color number at each image resolution (the initial Lenna image contains 52319 different colors, i.e., RGB triplets). We can observe that the watershed segmentation greatly reduces (by a factor of 15) the color number. However, since a quantization is usually applied on the input image as indicated at the beginning of this section, the difference appears not on the color number but rather on the quantized color distributions, as illustrated in Fig. 6(b). As we can notice in left column of Fig. 7, the watershed-based additional step introduces changes in particular on the object borders. Moreover, these changes appear more on a region-basis than on a pixel-basis, thus asserting the effect of the segmentation step. These interresolution differences lead to different evolutions of color distributions, see right column of Fig. 7.

IV. Experimental Evaluation

A. Setup

The retrieval tests that have been carried out have served multiple purposes. First they have been used in order to verify the practical interest of the presented morphological color descriptors, as well as to determine the optimal color space and quantization couple for this task. To this end, a total of 3000 images from three different sources have been used [49]–[51]. This set contained 16 semantic categories of 100 images each, along with 1400 bulk images, in order to simulate real-life retrieval from an unorganized database. Examples from each category are given in Fig. 8. Furthermore, in order to obtain more reliable estimates, each image of the 16 categories served as the query subject in

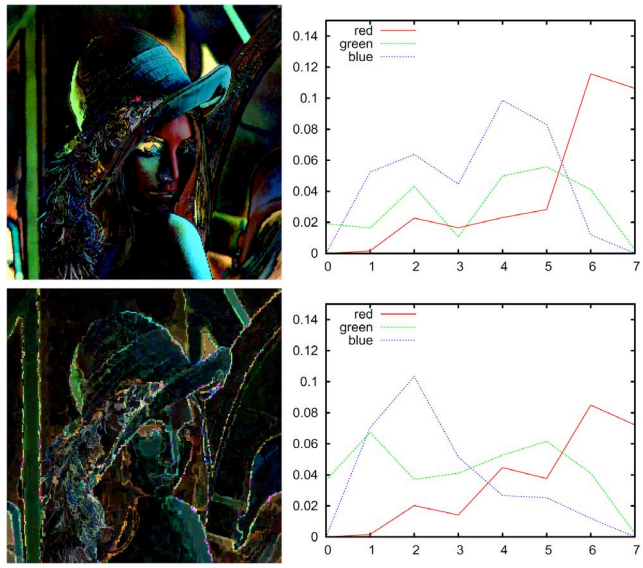

Fig. 7. Amount of differences accumulated over the five different resolutions using levelings only (top) and levelings followed by watersheds (bottom). The visual differences (left) lead to differences in the color distributions (right).

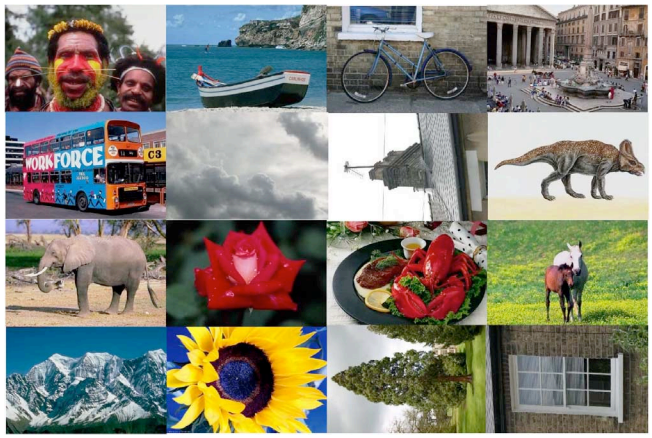

Fig. 8. Representative category examples of the image database used for color descriptor comparisons. From top-left to bottom-right: Africa, beach, bicycles, building, bus, clouds, chimneys, dinosaur, elephant, flower, food, horse, mountain, sunflower, tree, and window.

turn, making a total of 1600 queries. From the results of which the precision versus recall charts have been computed, as well as ANMRR values that provides an overall rating of performance.

ANMRR stands for *average normalized modified retrieval rank* and is the MPEG-7 retrieval effectiveness measure commonly accepted in the CBIR community [20]. More precisely, this measure has been introduced in order to overcome problems such as those related to queries with varying ground truth set sizes. In particular, given a query q, assume that the kth ground truth image is retrieved at $\mathrm{Rank}(k)$. Then a number $\mathrm{K}(q)$ is defined, which denotes the ranks that are considered as feasible in terms of retrieval evaluation. $\mathrm{K}(q)$ is often set as twice the size of the ground truth set $\mathrm{NG}(q)$ associated with the query under consideration. Hence, $\mathrm{Rank}^*(k)$ is defined, which represents the penalty attributed to a retrieved item

$$\mathrm{Rank}^*(k) = \begin{cases} \mathrm{Rank}(k), & \text{if } \mathrm{Rank}(k) \leq \mathrm{K}(q) \\ 1.25\mathrm{K}(q), & \text{if } \mathrm{Rank}(k) > \mathrm{K}(q) \end{cases}. \quad (25)$$

Thus, one gets the average rank (AVR) for a query q

$$\mathrm{AVR}(q) = \frac{1}{\mathrm{NG}(q)} \sum_{k=1}^{\mathrm{NG}(q)} \mathrm{Rank}^*(k). \tag{26}$$

Skipping the intermediate notions, we can directly define the ANMRR as

$$\mathrm{ANMRR} = \frac{1}{\mathrm{NQ}} \sum_{q=1}^{\mathrm{NQ}} \frac{\mathrm{AVR}(q) - 0.5(1 + \mathrm{NG}(q))}{1.25\mathrm{K}(q) - 0.5(1 + \mathrm{NG}(q))} \tag{27}$$

where NQ is the number of queries. Thus, ANMRR can provide values between 0 for best results (i.e., all images of the ground truth of the queries have been retrieved), and 1 for worst results (i.e., none of the ground truth images of the queries has been retrieved).

It should be additionally noted that for the charts the first retrieved image was always ignored as it represents the query image itself. In our tests, the proposed morphological color descriptors have been compared against the standard histogram, the autocorrelogram (AC) [31], the superiority of which with respect to the histogram has been shown by multiple comparative studies [22], [25], the color structure descriptor (CSD) [20] of the MPEG-7 standard and color distribution entropy (CDE) [21].

Moreover, a question that arises at this point is "why use a nonstandard image database?". Indeed, our initial intent was in the opposite direction; however, it became soon clear that contemporary image collections, such as Caltech-256 [50] are rather unsuitable for this particular testing suite, in the sense that they require descriptors capable of taking into account multiple visual dimensions (e.g., color, shape, etc.) simultaneously, thus rendering them inappropriate for the present case where we wish to focus on color, and color only. Of course this also represents a limit for this series of tests, as the results rest valid for collections with a certain level of color separability among categories.

B. Test Results

1) Color Space and Quantization: According to previous comparative studies [22] and the MPEG-7 standard [20], polar color spaces in general outperform most of their alternatives in the context of content description, in combination with different quantization models. Considering, however, the design problems of these spaces (Section II-A), and the alternative formulations that have been proposed, it has been considered appropriate to test their effectiveness in order to determine the most suitable color space along with its quantization model for the image database under consideration.

To this end, we have employed color histograms along with RGB, $\mathrm{L^*a^*b^*}$, HSV, and LSH with three different uniform quantization models, namely 8 (8-8-8), 6 (6-6-6), and 4 (4-4-4) bins per channel. The resulting ANMRR values are given in Table I. Judging from the obtained results, there are primarily two remarks to be made: first, the general superiority of LSH with respect to its counterparts, a result which confirms previous studies [25]. And additionally, one can observe the relatively light influence of histogram bin numbers. As a matter of fact, even with eight times less colors, the performance of the histograms decreases only by 4% for the best color space under study and less than 6% for the others.

TABLE I
ANMRR VALUES FOR DIFFERENT QUANTIZATION MODELS (HISTOGRAM BINS) AND COLOR SPACES

Color spaces	8-8-8 (512)	6-6-6 (216)	4-4-4 (64)
RGB	0.4993	0.5042	0.5478
$\mathrm{L^*a^*b^*}$	0.5544	0.5718	0.6127
HSV	0.4912	0.4998	0.5518
LSH	0.4759	0.4824	0.5158

TABLE II
ANMRR VALUES FOR DIFFERENT EXPRESSIONS OF BRIGHTNESS USING 256 BIN BRIGHTNESS HISTOGRAMS

Value	Intensity	Luminance
0.707	0.6843	0.7086

TABLE III
ANMRR VALUES FOR DIFFERENT EXPRESSIONS OF SATURATION USING 256 BIN SATURATION HISTOGRAMS

Luminance dependent	Independent
0.7053	0.6655

TABLE IV
ANMRR VALUES FOR SATURATION WEIGHTED AND UNWEIGHTED 256 BIN HUE HISTOGRAMS

Saturation weighted	unweighted
0.5892	0.6275

Based on the performance of the two polar color spaces, from this point on we focus on the optimization of their arguments. For instance, which brightness expression is most adequate for this task? Value (maximum of R, G, B), intensity (average of R, G, B), or luminance (perceptually weighted combination of R, G, and B)? Table II presents the results obtained using a 256 bin brightness histogram with the aforementioned expressions. According to the obtained results, the relatively simple expression of red green blue average, provides an overall better performance with this set.

Proceeding to the other two channels, as far as saturation is concerned, we test the brightness dependent version of HSV against the brightness independent definition of LSH, by means of a 256 bin saturation histogram. Table III shows the obtained ANMRR values. According to the results, brightness independence aids saturation's retrieval performance.

As to the hue component, we choose the implementation of LSH, and test the effect of using a saturation weighted hue histogram against a "raw" hue histogram, where the hue values of achromatic pixels take place as well. Table IV shows the obtained results. The weighting factor has indeed a positive effect.

In the light of these results, we opt for the LSH color space, equipped with the R, G, B average as brightness expression, and its hue weighted by its saturation. Furthermore, since

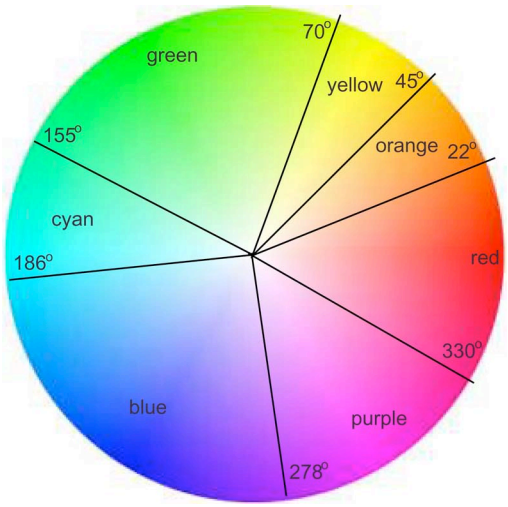

Fig. 9. Nonuniform hue circle quantization.

TABLE V
ANMRR VALUES FOR VARIOUS QUANTIZATION MODELS. NU STANDS FOR NONUNIFORM

Quantization model	Color number	ANMRR
3-3-7 (NU)	63	0.4908
3-3-8	72	0.5045
4-4-8	128	0.4912
3-3-12	108	0.4813
3-3-16	144	0.4800
4-4-12	192	0.4729
4-4-16	256	0.4717

the hue histogram is evidently more pertinent with respect to brightness and saturation, similarly to the general tendency [20], [23], nonuniform quantization of LSH is tested next. Besides, allowing a lower number of levels for brightness, has the additional advantage of limiting the effect of illumination variations. But the question is, how exactly should one quantize this space? Common models include 4-4-16 [20], 3-3-12 [25], as well as 3-3-9 [21]. Moreover one has also the option of quantizing the hue circle nonuniformly, according to [52], which is based on the fact that human color perception has a varying capacity of hue distinction. For instance, the average person can distinguish more hues of red than blue. This principle is illustrated in Fig. 9, and the quantization option is tested as 3-3-7 (NU). Table V summarizes the results obtained from various quantization models. Although in general the exact configuration has relatively small effect on the retrieval performance, as a practical compromise between color number (i.e., feature size) and effectiveness, the nonuniform 3-3-7 stands out. Hence, it will be subsequently used as the default quantization scheme, unless stated otherwise.

2) Descriptors: Having chosen the LSH color space with a nonuniform subquantization of type 3-3-7 [52] (see Fig. 9), we now continue to compare the color descriptors presented in Section III against some of the classical methods of color content

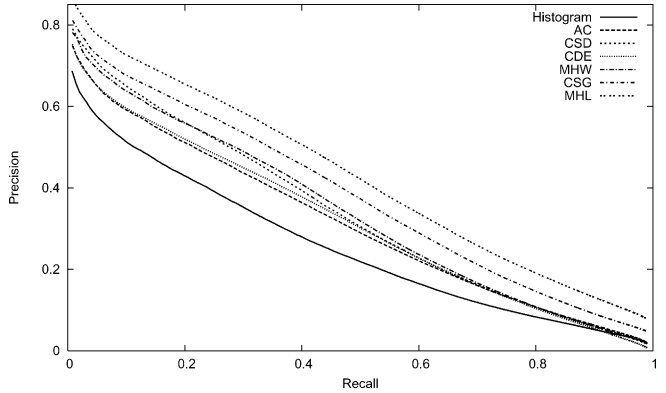

Fig. 10. Precision versus recall chart of the tested color descriptors, from worst to best descriptors: standard histogram, autcorrelogram (AC), color structure descriptor (CSD), color distribution entropy (CDE), multiresolution histograms with watersheds (MHW), color specific granulometry (CSG), multiresolution histogram with levelings (MHL).

description. As far as CSG is concerned, the projection of each quantized color within the 63 color set is computed using the distance between the color under consideration and the original unquantized image. The distance expression is set to a weighted combination of hue and luminance difference

$$\begin{aligned} \forall c_1 = \{h_1, s_1, l_1\}, c_2 = \{h_2, s_2, l_2\} \\ d(c_1, c_2) = (h_1 \div h_2) \times j(s_1, s_2) \\ + |l_1 - l_2| \times (1 - j(s_1, s_2)) \end{aligned} \tag{28}$$

where all color components have been normalized to [0,1], the weight $j(\cdot,\cdot)$ is given in (24) and $\div$ represents the standard hue distance defined in (5). Moreover, the granulometries have been computed using square shaped SE with 4 sizes, 1, 5, 9, and 13 pixels wide using the efficient algorithm of [53]. Thus, with $3 \times 3 \times 7 = 63$ colors, it leads to a feature vector of length $4 \times 63 = 252$. As to MHL, based on empirical observations it has been decided to use ASF (with opening first) in order to realize the levelings, in 4 different resolutions, with the same SE options as CSG. Levelings of the same setup have been also used along with MHW, prior to applying the watersheds. Consequently, all three operators lead to identical feature vector sizes.

On the other hand, as to their rivals, the standard color histogram is computed in LSH using the subquantization model 4-4-16 with histogram size 256. The AC is calculated with the same setup as in [25], where it is defined for the HSV color space in combination with a subquantization model of 12-3-3. Namely, with four distances (1,3,5,7), hence leading to a feature vector of length $108 \times 4 = 432$. For the CSD, we use the configuration presented in [20] but with the aforementioned color space related choices instead of the HMMD space. Consequently it provides a feature vector of the same length as the standard histogram. In order to calculate the CDE we follow the definition given in [21], with the number of radius quantization levels set to $N = 4$ which results in a description of length 252.

The precision versus recall charts resulting from the 1600 queries are shown in Fig. 10, whereas the ANMRR values are given in Table VI. As expected, the total lack of spatial information places the standard color histogram last, while considerable improvements are achieved by both AC and CDE that provide

TABLE VI
ANMRR VALUES FOR THE TESTED COLOR DESCRIPTORS

Histogram	AC	CSD	CDE	CSG	MHW	MHL
0.4717	0.4341	0.4132	0.4289	0.3935	0.4156	**0.3767**

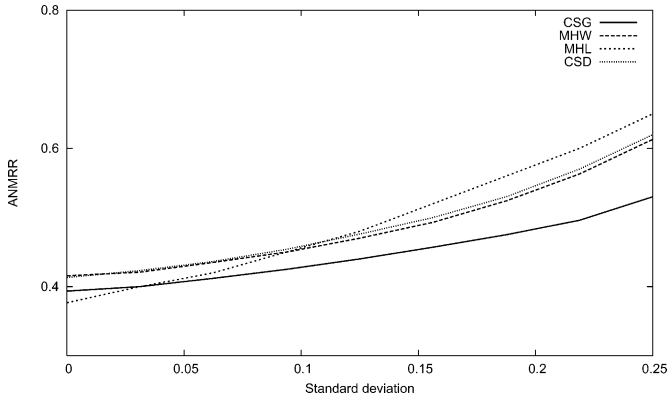

Fig. 11. Chart of ANMRR values with respect to various noise deviation levels of the tested color descriptors.

TABLE VII
RELATIVE COMPUTATION TIMES OF VARIOUS DESCRIPTORS TO THE STANDARD COLOR HISTOGRAM

Histogram	AC	CSD	CDE	CSG	MHW	MHL
1	127	89	9	548	470	443

likewise performances. Among the legacy descriptors, similarly to the study of Ojala *et al.* [23], the CSD gives the best retrieval results. As far as the proposed color description operators are concerned, with the exception of MHW, they all lead to superior performances, especially in terms of precision. In particular, we can observe that the MHW has a similar output with CSD, while both CSG and MHL outperform their counterparts, with the latter providing the best results. We now proceed to test their robustness against noise.

To test the noise robustness of the proposed descriptors, we have corrupted the images of our database with various levels of zero-mean additive Gaussian noise, and measured their retrieval performances. In particular, the images have been contaminated with noise in the RGB color space. The ANMRR values that have been obtained are shown in Fig. 11. This time they are compared only against CSD, as its noise robustness is known to be superior to its alternatives [20]. Judging from the obtained values, we can immediately remark the sensitivity of the previously outperforming MHL to noise levels, while MHW and CSD once more provide very similar outputs. CSG, however, exhibits a somewhat higher robustness. Further steps to improve their performance with corrupted image data could include the use of rank based morphological operators.

As to their computation times, they are given in Table VII with respect to that of a standard color histogram. Generally speaking all three morphology based approaches are significantly slower than their counterparts, nevertheless they still possess a certain margin for further efficiency optimization. Hence, one tends to conclude that they are unsuitable, at least in this form, for online retrieval systems. Nevertheless, we have not yet used all optimized versions of morphological operators during the elaboration of the proposed descriptors. A deep execuction analysis of our descriptors gives the following results. The main bottleneck within CSG is the closing by reconstruction step involved in the granulometry. Since we are using the efficient reconstruction algorithm from Vincent [53], most of the time is computed in the morphological closing operator itself. Possible ways of decreasing computation time are to involve efficient low-level (e.g., erosion/dilation) or high-level (e.g., granulometry) operators [54], perform SE decomposition to reduce the number of pixel comparisons, etc.As far as the mutiresolution histograms are concerned, the high computation time is due to the ASF and levelings operations. Nevertheless, it is possible to rely on other multiscale watershed segmentations to produce the scale-space from which is computed the histogram. Such efficient multiscale segmentations have focusing the attention of the mathematical morphology community for years [47], [48] and is still very topical [9].

V. CONCLUSION

This paper has focused on the application of the morphological framework to the problem of color description. In particular, the main properties of color from a descriptive point of view have been determined and a state-of-the-art ordering approach has been implemented for the extenstion of mathematical morphology to color images. Subsequently, three global descriptors have been proposed, focusing mainly on the integration of spatial information with spectral color distribution through morphological means. Specifically, the proposed approaches include the color specific granulometry, which provides a size distribution independently computed for each subquantized color, and two multiresolution histograms based on morphological levelings and watersheds. The tests that have followed, have provided results asserting their competitive performance with respect to known alternatives. Nevertheless, the relatively high computation time that is required prohibits their use with online retrieval systems, while also leaving a considerable margin for speed optimization. A the field of mathematical morphology offers numerous efficient algorithms, this issue is not so critical.

In conclusion, the proposed morphological descriptors possess mixed properties, and while providing a retrieval performance as well as noise robustness comparable to contemporary approaches, they do have still efficiency issues that need to be resolved if they are to be used along with online CBIR systems. Nevertheless, since the existence of efficient morphological algorithms will most probably greatly reduce the computation time of proposed descriptors, this step into the field of CBIR-oriented morphological image content description will serve as a basis for the subsequent development of more sophisticated operators, e.g., morphological color interest point detectors, multiscale watershed segmentations.

REFERENCES

[1] J. Serra, "Patent: "Automatic Scanning Device for Analyzing Textures"," France 23 273, Jul. 2, 1965a.

[2] G. Matheron, *Eléments Pour Une Théorie Des Milieux Poreux*. Paris, France: Masson, 1967.

[3] P. Soille, *Morphological Image Analysis: Principles and Applications*, 2nd ed. Berlin, Germany: Springer-Verlag, 2003.

[4] B. Naegel, N. Passat, and C. Ronse, "Grey-level hit-or-miss transforms—Part II: Applications to angiographic image processing," *Pattern Recognit.*, vol. 40, no. 2, pp. 648–658, Feb. 2007.

[5] S. Lefèvre, J. Weber, and D. Sheeren, "Automatic building extraction in VHR images using advanced morphological operators," in *Proc. IEEE/ISPRS Joint Workshop on Remote Sensing and Data Fusion Over Urban Areas*, Paris, France, Apr. 2007.

[6] J. Weber and S. Lefèvre, "A multivariate hit-or-miss transform for conjoint spatial and spectral template matching," in *Proc. IEEE Int. Conf. Image and Signal Processing*, Cherbourg, France, Jul. 2008, vol. 5099, pp. 226–235, ser. Lecture notes in computer science.

[7] J. Angulo, "Morphologie Mathématique et Indexation d'Images Couleur. Application à la Microscopie en Biomédicine," Ph.D. dissertation, Ecole des Mines, Paris, France, 2003.

[8] M. H. F. Wilkinson and F. Tushabe, "Content-based image retrieval using shape-size pattern spectra," in *CLEF Workshop*, A. Nardi and C. Peters, Eds., Budapest, Hungary, 2007.

[9] R. Lerallut, "Modélisation et Interprétation d'Images à l'Aide de Graphes," Ph.D. dissertation, Ecole des Mines, Paris, France, 2006.

[10] I. Pratikakis, I. Vanhamel, H. Sahli, B. Gatos, and S. Perantonis, "Watershed-driven region-based image retrieval," in *Mathematical Morphology: 40 Years on*, ser. Computational Imaging and Vision, C. Ronse, L. Najman, and E. Decencière, Eds. Dordrecht, The Netherlands: Springer-Verlag, 2005, vol. 30, pp. 207–216.

[11] F. A. Andaló, P. A. V. Miranda, R. D. S. Torres, and A. X. Falcão, "A new shape descriptor based on tensor scale," in *Proc. 8th Int. Symp. Mathematical Morphology*, U. M. Braga-Neto , G. J. F. Bannon, and J. Barrera, Eds., Rio de Janeiro, Brazil, Oct. 2007, vol. 1, pp. 141–152, INPE.

[12] H. J. A. M. Heijmans, *Morphological Image Operators*, ser. Advances in Electronics and Electron Physics Series. Boston, MA: Academic, 1994.

[13] E. Aptoula and S. Lefèvre, "A comparative study on multivariate mathematical morphology," *Pattern Recognit.*, vol. 40, no. 11, pp. 2914–2929, Nov. 2007.

[14] A. Hanbury and J. Serra, "Colour image analysis in 3d-polar coordinates," in *Proc. DAGM*, Magdeburg, Germany, Sep. 2003, vol. 2781, pp. 124–131, ser. Lecture notes in computer science, Springer-Verlag.

[15] A. Hanbury, "Constructing cylindrical coordinate colour models," *Pattern Recognit. Lett.*, vol. 4, no. 29, pp. 494–500, Mar. 2008.

[16] J. Angulo, "Unified morphological color processing framework in a lum/sat/hue representation," in *Mathematical Morphology: 40 Years On*, ser. Computational Imaging and Vision, C. Ronse, L. Najman, and E. Decencière, Eds. Dordrecht, The Netherlands: Springer-Verlag, 2005, vol. 30, pp. 387–396.

[17] J. Angulo and J. Serra, "Modelling and segmentation of colour images in polar representations," *Image Vis. Comput.*, vol. 25, no. 4, pp. 475–495, Apr. 2007.

[18] E. Aptoula and S. Lefèvre, "On lexicographical ordering in multivariate mathematical morphology," *Pattern Recognit. Lett.*, vol. 29, no. 2, pp. 109–118, Jan. 2008.

[19] A. Hanbury and J. Serra, "Morphological operators on the unit circle," *IEEE Trans. Image Process.*, vol. 10, no. 12, pp. 1842–1850, Dec. 2001.

[20] B. S. Manjunath, J. R. Ohm, V. V. Vasudevan, and A. Yamada, "Color and texture descriptors," *IEEE Trans. Circuits Syst. Video Technol.*, vol. 11, no. 6, pp. 703–715, Jun. 2001.

[21] J. Sun, X. Zhang, J. Cui, and L. Zhou, "Image retrieval based on colour distribution entropy," *Pattern Recognit. Lett.*, vol. 27, no. 10, pp. 1122–1126, Oct. 2006.

[22] W. Y. Ma and H. J. Zhang, "Benchmarking of image features for content-based image retrieval," in *Proc. 32nd Asilomar Conf. Signals, Systems, Computers*, Pacific Grove, CA, Nov. 1998, vol. 1, pp. 253–257.

[23] T. Ojala, T. Maenpaa, M. Pietikainen, J. Viertola, J. Kyllonen, and S. Huovinen, "Outex: New framework for empirical evaluation of texture analysis algorithms," in *Proc. 16th ICPR*, Quebec City, Canada, Aug. 2002, vol. 1, pp. 701–706.

[24] G. D. Finlayson, S. Hordley, G. Schaefer, and G. Y. Tian, "Illuminant and device invariant colour using histogram equalisation," *Pattern Recognit.*, vol. 38, no. 2, pp. 179–190, Feb. 2005.

[25] T. Ojala, M. Rautiainen, E. Matinmikko, and M. Aittola, "Semantic image retrieval with HSV correlograms," in *Proc. 12th Scandinavian Conf. Image Analysis*, Bergen, Norway, 2001, pp. 621–627.

[26] J. Angulo and J. Serra, "Morphological color size distributions for image classification and retrieval," in *Proc. Int. Conf. Advanced Concepts for Intelligent Vision Systems*, Ghent, Belgium, Sep. 2002, pp. 46–53.

[27] G. Louverdis, I. Andreadis, and P. Tsalides, "Morphological granulometries for color images," in *Proc. 2nd Hellenic Conf. Artificial Intelligence*, Thessaloniki, Greece, Apr. 2002, pp. 333–342.

[28] G. Matheron, *Random Sets and Integral Geometry*. New York: Wiley, 1975.

[29] E. R. Urbach, J. B. T. M. Roerdink, and M. H. F. Wilkinson, "Connected shape-size pattern spectra for rotation and scale-invariant classification of gray-scale images," *IEEE Trans. Pattern Anal. Mach. Intell.*, vol. 29, no. 2, pp. 272–285, Feb. 2007.

[30] M. H. F. Wilkinson, "Generalized pattern spectra sensitive to spatial information," in *Proc. 16th ICPR*, Quebec City, Canada, Aug. 2002, vol. 1, pp. 21–24.

[31] J. Huang, S. R. Kumar, M. Mitra, W. J. Zhu, and R. Zabih, "Image indexing using color correlogram," in *Proc. IEEE Int. Conf. Computer Vision and Pattern Recognition*, San Juan, PR, Jun. 1997, pp. 762–768.

[32] S. Lefèvre, "Beyond morphological size-distribution," *J. Electron. Imag.*, vol. 18, no. 1, 2009, article 013010.

[33] F. Sand and E. Dougherty, "Robustness of granulometric moments," *Pattern Recognit.*, vol. 32, pp. 1657–1665, 1999.

[34] M. J. Swain and D. H. Ballard, "Color indexing," *Int. J. Comput. Vis.*, vol. 7, no. 1, pp. 11–32, Nov. 1991.

[35] A. Rao, R. K. Srihari, and Z. Zhang, "Spatial color histograms for content-based image retrieval," in *Proc. 11th IEEE Int. Conf. Tools With Artificial Intelligence*, Chicago, IL, Nov. 1999, pp. 183–186.

[36] E. Hadjidemetriou, M. D. Grossberg, and S. K. Nayar, "Multiresolution histograms and their use for recognition," *IEEE Trans. Pattern Anal. Mach. Intell.*, vol. 26, no. 7, pp. 831–847, Jul. 2004.

[37] S. Lazebnik, C. Schmid, and J. Ponce, "Beyond bags of features: Spatial pyramid matching for recognizing natural scene categories," in *Proc. Int. Conf. Computer Vision and Pattern Recognition*, New York, Jun. 2006, vol. 2, pp. 2169–2178.

[38] A. K. Jain and F. Farroknia, "Unsupervised texture segmentation using Gabor filters," *Pattern Recognit.*, vol. 24, no. 12, pp. 1167–1186, 1991.

[39] M. Popovic, "Texture analysis using 2d wavelet transform: Theory and applications," in *Proc. 4th Int. Conf. Telecommunications in Modern Satellite, Cable and Broadcasting Services*, Nis, Serbia, Oct. 1999, vol. 1, pp. 149–158.

[40] F. Meyer and P. Maragos, "Nonlinear scale space representation with morphological levelings," *J. Vis. Commun. Image Represent.*, vol. 11, no. 2, pp. 245–265, June 2000.

[41] C. Vachier, "Morphological scale-space analysis and feature extraction," in *Proc. Int. Conf. Image Processing*, Thessaloniki, Greece, Oct. 2001, vol. 3, pp. 676–679.

[42] F. Meyer, "Levelings, image simplification filters for segmentation," *J. Math. Imag. Vis.*, vol. 20, pp. 59–72, 2004.

[43] C. Gomila and F. Meyer, "Levelings in vector spaces," in *Proc. IEEE Conf. Image Processing*, Kobe, Japan, Oct. 1999.

[44] J. Angulo and J. Serra, "Morphological coding of color images by vector connected filters," in *IEEE Proc. 7th Int. Symp. Signal Processing and its Applications (ISSPA'2003)*, Paris, France, Jul. 2003, vol. 1, pp. 69–72.

[45] K. Karantzalos, D. Argialas, and N. Paragios, "Comparing morphological levelings constrained by different markers," in *Proc. 8th Int. Symp. Mathematical Morphology*, U. M. Braga-Neto, G. J. F. Bannon, and J. Barrera, Eds., Rio de Janeiro, Brazil, Oct. 2007, vol. 1, pp. 113–124, INPE.

[46] K. Grauman and T. Darrell, "Benchmarking of image features for content-based image retrieval," in *Proc. Int. Conf. Computer Vision*, Beijing, China, Oct. 2005, vol. 2, pp. 1458–1465.

[47] S. Beucher, "Watershed, hierarchical segmentation and waterfall algorithms," in *Mathematical Morphology and its Applications to Image Processing*, J. Serra and P. Soille, Eds. Boston, MA: Kluwer, 1994, pp. 69–76.

[48] L. Najman and M. Schmitt, "Geodesic saliency of watershed contours and hierarchical segmentation," *IEEE Trans. Pattern Anal. Mach. Intell.*, vol. 18, no. 2, pp. 1163–1173, Feb. 1996.

[49] Corel Corporation, Corel Gallery Images [Online]. Available: http://www.corel.com

[50] G. Griffin, A. Holub, and P. Perona, Caltech-256 Object Category Dataset California Inst. Technol., Tech. Rep. 7694, 2007 [Online]. Available: http://authors.library.caltech.edu/7694

[51] *Google Search Engine*, [Online]. Available: http://www.google.com

[52] H. Y. Lee, H. K. Lee, and Y. H. Ha, "Spatial color descriptor for image retrieval and video segmentation," *IEEE Trans. Multimedia*, vol. 5, no. 3, pp. 358–367, May 2003.

[53] L. Vincent, "Morphological grayscale reconstruction in image analysis: Applications and efficient algorithms," *IEEE Trans. Image Process.*, vol. 2, no. 2, pp. 176–201, Apr. 1993.
[54] L. Vincent, "Granulometries and opening trees," *Fundam. Inf.*, vol. 41, no. 1–2, pp. 57–90, 2000.

Erchan Aptoula received the B.Sc. degree in computer engineering from Galatasaray University, Istanbul, Turkey, in 2004, the M.Sc. and Ph.D. degrees in computer science from Louis Pasteur University, Strasbourg, France, in 2005 and 2008. His doctoral work focused on color mathematical morphology applied to content-based image retrieval.

Apart from morphological analysis, his interests include multispectral image processing, pattern recognition, and machine learning.

Sébastien Lefèvre received the M.Sc. and Eng. degrees in computer engineering from the University of Technology of Compiègne, France, in 1999, and the Ph.D. degree in computer science from the University of Tours, France, in 2002.

He is currently an Assistant Professor in the Department of Computer Science and the LSIIT, University Louis Pasteur, Strasbourg. His research interests are in image/video processing using mainly mathematical morphology with applications in remote sensing, astronomical and medical imaging, and content-based image/video retrieval.